Enhanced tribological and corrosion properties of multilayer ta-C films via alternating sp^3 content

Jing Wei[a,b], Hanchao Li[a,c], Linlin Liu[a], Peng Guo[a], Peiling Ke[a,b], Aiying Wang[a,b,*]

[a] Key Laboratory of Marine Materials and Related Technologies, Zhejiang Key Laboratory of Marine Materials and Protective Technologies, Ningbo Institute of Materials Technology and Engineering, Chinese Academy of Sciences, Ningbo 315201, China
[b] Center of Materials Science and Optoelectronics Engineering, University of Chinese Academy of Sciences, Beijing 100049, China
[c] School of Physical Science and Technology, Shanghai Tech University, Shanghai 201210, China

ARTICLE INFO

ABSTRACT

Multilayer tetrahedral amorphous carbon (ta-C) films comprising alternating layers of different sp^3 contents have been fabricated by periodically adjusting the bias voltage of filtered cathodic vacuum arc (FCVA) system. The microstructure, tribological and corrosion behaviors of the multilayer ta-C films deposited on YG6 cemented carbide were systematically investigated. Results showed that the multilayer structure effectively reduced the residual stress and restrained spalling of ta-C film, which frequently occurred in single-layer structure. The hardness and Young's modulus of multilayer ta-C films decreased with diminishing sp^3 content of soft sublayer. Compared to the YG6 substrate, multilayer ta-C films exhibited much lower friction coefficient between 0.06 and 0.08 and effectively reduced the wear rate. Multilayer ta-C film deposited at bias voltage alternating between −50 V and –150 V (M-1 film) had the lowest friction coefficient of 0.06 and the lowest wear rate of 2.87×10^{-7} mm^3/N m. The difference in anti-wear performance among the multilayer ta-C films was associated with the ratio of hardness to elastic modulus (H/E ratio). The electrochemical corrosion test confirmed the effective corrosion protection provided by the multilayer ta-C films, and the M-1 film obtained the highest polarization resistance. Judging from electrochemical impedance tests, the existence of some extent of micro-defects could be the main factor limiting the electrochemical corrosion performance of the multilayer ta-C films.

1. Introduction

In recent years, engineering materials suffering from aggressive medium and mechanical loading have aroused widespread concerns [1–4]. Combined protection against friction and corrosion is an urgent need to improve the reliability and life-time of engineering components under harsh and complicated working conditions.

Cemented carbide comprised of hard ceramic phase (WC) and metallic binder (e.g., Co, Ni) has been found its use in various engineering components, such as cutting tools, saw blades, valves and jet nozzles, due to its excellent hardness and toughness. However, for some special applications, such as wood cutting, petroleum transportation and mining, the tungsten carbide has to not only deal with mechanical wear, but also suffer corrosive attack from cutting fluid, mine water and seawater [5–7]. Unfortunately, tungsten carbide itself lacks effective wear resistance in corrosive working conditions [8].

Protective coating serves as an important role in surface

modification of materials. One of the attractive candidate is diamond-like carbon (DLC) film, which is a metastable form of amorphous carbon containing sp^2 and sp^3-hybridized carbon and hydrogen. In DLC family, tetrahedral amorphous carbon (ta-C) has high content of sp^3 bonds, and no hydrogen element is embedded in its carbon network, which endows ta-C film with high density, excellent wear resistance and chemical inertness [9]. At present, ta-C film has been employed in mechanical protection of cemented carbide [10–12]. However, its corrosion performances on cemented carbides have received less attention, mainly due to the limited thickness of ta-C film resulting from high stress level during growth.

Interlayer deposition, doping elements and multilayer structure are effective methods to reduce the residual stress of ta-C film [13–16]. Nevertheless, the transition layer and element doping would complicate the process and introduce heterogeneous elements. Many literatures have elucidated that alternating hard and soft multilayer structure could remarkably reduce stress. In arc deposition, the bias voltage could

effectively regulate the sp^3 bond content and tailor the hardness [17–24]. For example, Zhu et al. [20] have reported that the sp^3 fraction could be tailored from 82% to 56% by changing the bias voltage between 0 V and –200 V, while the corresponding hardness evolved from 51 GPa to 31 GPa. Zavaleyev et al. [23] have demonstrated that regulating the bias voltage in the range of −25 V to −200 V leads to the modification of sp^3 content and hardness of the deposited ta-C films from 35% and 18 GPa to 63% and 50 GPa, respectively. By periodically adjusting the deposition bias voltage, multilayer DLC films with alternating high and low sp^3 content (hard and soft) layers can be obtained. At present, the research of multilayer DLC film mainly focuses on microstructure characterization and mechanical properties [25–28]. Xu et al. [25,26] demonstrated that the reduction of modulation ratio resulted in lower sp^3 content and hardness of the multilayer DLC films, and sample with modulation ratio of 1:1 obtained the best wear resistance mainly due to balance between hardness and residual stress. Finite element model could accurately simulate the film deformation, providing guidance for the optimization process. Han et al. [28] found that the graded multilayer ta-C films had excellent scratch resistance and adhesive strength, which possibly originated from the storage of elastic energy by sublayer's interface during scratch loading. However, there still lack research for multilayer DLC film in terms of the combined anti-wear and electrochemical corrosion behaviors.

In present work, we construct multilayer ta-C films by alternating high-sp^3-content layer and low-sp^3-content layer, aiming to optimize its performance under complicated working conditions and to figure out the role of multilayer structure on its tribological and electrochemical corrosion properties.

2. Experimental

2.1. Film preparation

YG6 cemented carbide with a size of 15 mm × 15 mm, P-type silicon (100) wafers with thickness of 280 ± 15 um and 545 ± 15 um were selected as substrates. The ta-C films were deposited using a self-designed 45 degree double-bent filtered cathodic vacuum arc (FCVA) system, as shown in Fig. 1. The magnetic filter composed of 45 degree double-bent stainless steel tube and permanent magnet coil (PM), source magnetic coil (SM), extraction magnetic coil (EM), bending magnetic coil (BM) and output magnetic coil (OM) could realize effective filtration of large macro-particles. The polarity-direction of the

respective field coils is showed in the insert diagram of Fig. 1. The current of SM, EM, BM and OM were set as 5.0 A, 4.5 A, 4.5 A and 4.5 A, respectively. The duct diameter of double bent FCVA was 16 cm. The magnetic field strength inside the duct was between 43 mT and 108 mT, and the magnetic induction intensity on the axis of the duct was mainly between 53 and 94 mT. The spatial distribution of magnetic field in the duct obtained by simulation was shown in Fig. S1. A trapezoidal high purity graphite (99.999%) with diameters of Φ_{max}70 mm and Φ_{min}60 mm was used as target. The arc was triggered by mechanical W needle. A positive bias voltage of 20 V was applied to the duct and the arc current was kept at 60 A. Four scanning coils were installed at the outlet of the magnetic filter duct, in order to increase deposition area and improve the uniformity of the deposited film. The magnetic field distribution of the scanning coil is controlled by adjusting the amplitude and frequency of AC power supply. The frequencies of beam scanning both in X axis and Y axis are 8 Hz. In order to regulate the carbon ion energy, specific substrate bias voltages (−50 V, −150 V, −250 V, −350 V) were applied. The arc and bias voltage were both supplied by pulsed DC power.

The pumping system was comprised of mechanical pump and turbomolecular pump. When the chamber was evacuated to a vacuum of 3.0×10^{-3} Pa, the substrates were firstly cleaned by arc plasma etching at −300 V for 10 min, then ta-C films were deposited under specific substrate bias voltages. The Ar flow rate for arc plasma etching and film deposition processes were 5.0 sccm and 1.5 sccm, respectively. The pressure during etching and deposition were 0.01 Pa and 0.04 Pa, respectively. As a preliminary experiment, single-layer ta-C films under the substrate bias voltages of −50 V, −150 V, −250 V, −350 V were systematically studied. The deposition rate decreased gradually from 12.4 to 4.3 nm/min with increasing bias voltage from −50 V to −350 V, as shown in Fig. S2. Then multilayer ta-C films with high-sp^3-content layer alternated with low-sp^3-content layer were deposited by varying the substrate bias voltage periodically. The modulation ratio of the hard and soft layers was set as 1:1 and the modulation period was about 50 nm. The performances of the multilayer system could be tailored by regulating components of adjacent layers. The first layer contacted with the substrate was set as a low-sp^3-content ta-C layer in order to improve the film-substrate adhesion, while a high-sp^3-content ta-C layer was always selected as the top layer for wear protection. The top hard layer could provide high load carry capacity and contribute to long wear life. The film thickness was kept almost constant by varying the deposition time for each case.
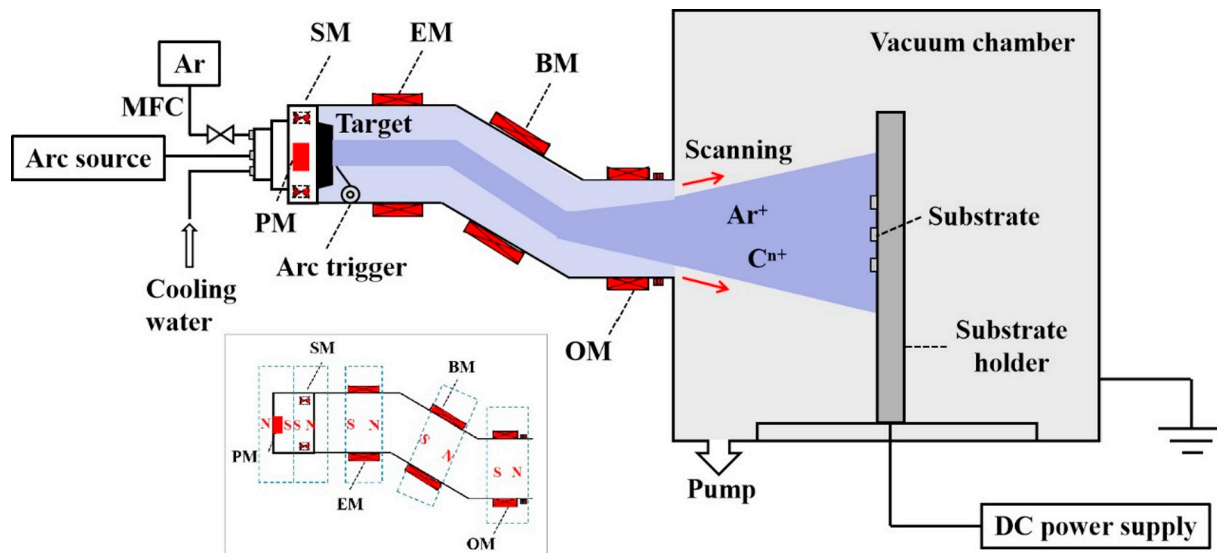

Fig. 1. Schematic diagram of FCVA system (Insert diagram shows the polarity-direction of the respective field coils).

2.2. Microstructural characterization

X-ray photoelectron spectroscopy (XPS, Axis ultradld, Japan) with monochromatic Al X-ray source was employed to analyze the chemical bonding ta-C films. The XPS device was equipped with electron neutralizing gun, which neutralized the charge on the sample surface using a low-energy electron beam. The emitted photoelectrons were detected using a concentric hemispherical analyzer at a pass energy of 160 eV for the survey scan and 20 eV for the high resolution XPS peaks. The sample surface was etched by Ar^+ ion beam before measurement to remove the contaminants. The small spot XPS depth profiling was further utilized to characterize the distribution of sp^3 content with depth. Argon ion etching conditions for removing the contamination were: Ar^+ energy of 2 keV, time duration of 1 min. The etching conditions for small spot XPS depth profiling were: X-ray spot of 150×1000 mm2, Ar^+ energy of 2 keV, testing every 2 min of etching. The energy resolution of the XPS instrument was 0.48 eV in term of Ag 3d5/2 (FHMW). The binding energies were referenced with C 1s peak at 284.6 eV. The fitting process of C 1s spectra was provided in the supporting information S3. The field emission scanning electron microscopy (FE-SEM, Hitachi S-4800, Japan) was employed to analyze the surface and cross-sectional morphology of the multilayer ta-C films. High-resolution transmission electron microscopy (TEM, Tecnai F20, US), with a point-to-point resolution of 0.24 nm, was used to characterize the microstructure. The TEM sample was prepared by Focused Ion Beam (FIB) instrument (Carl Zeiss, Auriga). Electron energy loss spectroscopy (EELS) was acquired by scanning transmission electron microscope (STEM, Tecnai F20, US) operated at acceleration voltage of 200 kV, using a CCD camera (2048×2048 pixels) behind the Gatan imaging filter. The convergence and collection semi-angle were set at 25 and 60 mrad, respectively. The energy resolution, determined from the full width of half maximum of the zero-loss peak, was 0.64 eV. The typical acquisition times for C-K edge and low-loss spectra were 0.01 and 0.005 s, respectively. Highly oriented pyrolytic graphite (HOPG, 100% sp^2-C bonds) was selected as a standard for quantitative analysis of carbon bonding. The processing of C-K edge spectra follows the standard procedure, i.e., background subtraction by power-law model, removing the plural scattering using the Fourier-ratio deconvolution with the relevant low-loss spectra, spectra calibration by shifting the π^* peak to 285 eV. Raman spectroscopy (Renishaw inVia-reflex, UK) with a wavelength of 532 nm was used to measure the atomic bonds of the films before and after tribological test at a detecting range from 800 to 2000 cm^{-1}. The nano-indenter (MTS-G200) in continuous stiffness measurement mode was used to characterize the mechanical properties. The indentation depths were about 180 nm. The average values of hardness and elastic modulus in the stable region of 50–100 nm were

selected as the test results. Six indentations were done for each sample to ensure repeatability. A laser tester (JLCST022, J&L Tech) was utilized to define the film/substrate curvature, then the residual stress was further calculated through Stoney equation.

2.3. Tribological tests

Dry friction performance was evaluated by a reciprocating ball-on-disk tribo-meter (UMT-3) with Al_2O_3 ball (6 mm in diameter) as the counterpart at room temperature. The applied load, stroke length and sliding frequency were 5 N, 5 mm and 2 Hz, respectively. Each test lasted for 900 s. At least three friction tests were conducted for each sample to ensure repeatability. After friction tests, a surface profilometer (Alpha Step-IQ) was employed to measure the wear track profiles. The wear rate of each sample was calculated by the following equation:

$$K = \frac{V}{F \times L} \tag{1}$$

where V is the wear loss of the film in mm^3, F is the applied normal load in N and L is the sliding distance in m [24]. The field emission scanning electron microscopy (FE-SEM, FEI Quanta FEG 250) equipped with X-ray energy dispersive spectroscopy (EDS) was applied to characterize the wear tracks after friction test.

2.4. Electrochemical corrosion studies

Electrochemical corrosion performance was evaluated by a three-electrode electrochemical system in 3.5 wt% NaCl solution at room temperature. Platinum mesh, KCl saturated silver/silver chloride (Ag/AgCl) electrode, the ta-C film coated and uncoated YG6 samples were employed as counter, reference and working electrode, respectively. The exposed area of each sample to the electrolyte was 1.0 cm^2. Before measurement, the open circuit potential (OCP) was monitored for 1 h to establish an equilibrium. Electrochemical impedance spectroscopy (EIS) was conducted over a frequency range from 100 kHz to 10 mHz with 10 mV sinusoidal perturbation. In potentiodynamic polarization tests, the potential was swept from -0.6 V to 1.5 V at a scanning rate of 0.5 mV/s. All tests were repeated three times for each sample. The acquired data were analyzed using Modulab and ZSimpWin software.

3. Results and discussion

3.1. Film characterization

The XPS tests were firstly employed to characterize the sp^3 content
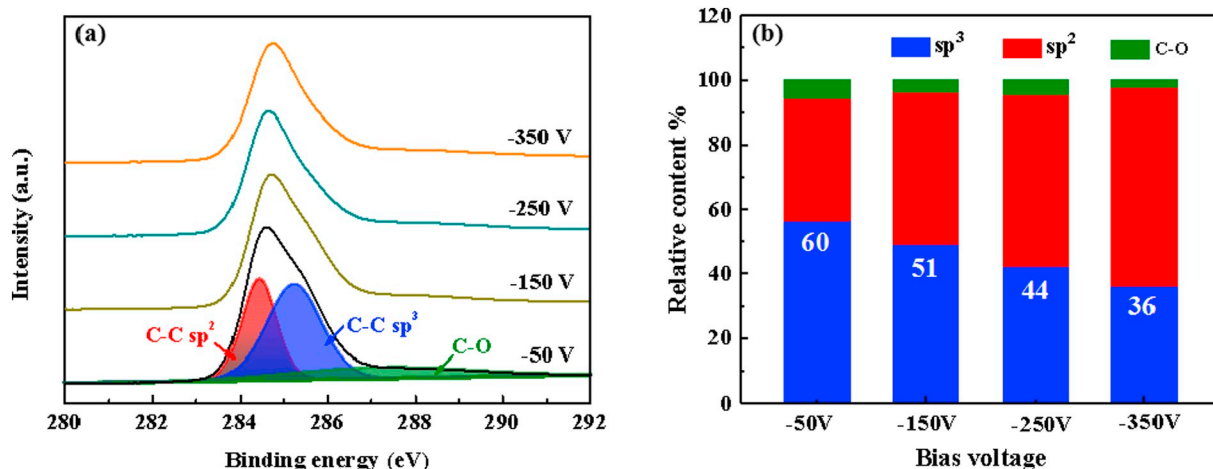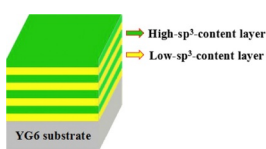

Fig. 2. (a) The XPS C1s core level spectra and (b) sp^3 content of single-layer ta-C films under different bias voltages.

Table 1
Specific information of the designed films.

Samples	Bias voltage (V)	sp³ content (at.%)	Thickness (nm)	
S-1	−50	60	230	
M-1	−150/−50	51/60	245	
M-2	−250/−50	44/60	261	
M-3	−350/−50	36/60	221	

of single-layer ta-C films under various bias voltage. As shown in Fig. 2(a), the C 1s spectra were deconvolved into three peaks located at 284.3 ± 0.2 eV, 285.2 ± 0.2 eV and 286.5 ± 0.3 eV, which originate from C−C sp² bond, C−C sp³ bond and C−O bond, respectively [29]. The obtained sp³ contents are further depicted in Fig. 2(b), which clearly shows that adjusting the bias voltage from −50 V to −350 V leads to monotonous decrease of the sp³ content from 60% to 36%.

Based on the above results, multilayer ta-C films with high-sp³-content layer (bias voltage of −50 V) alternated with low-sp³-content layer (bias voltage of −150 V/−250 V/−350 V) were designed and prepared, which were labelled as M-1, M-2, M-3, respectively. The single-layer ta-C film with the same thickness deposited at −50 V, labelled as S-1, served as a contrast sample. Specific information of the designed films is shown in Table 1. The film thickness of each sample was controlled around 240 ± 20 nm (Fig. S3).

It is worth noting that the S-1 film peeled off from the YG6 substrate (Fig. S4), while the multilayer films retained integrity without visible delamination. Meanwhile, a smooth surface of multilayer ta-C films could be obtained due to the effective filtration of macroparticles by magnetic filter system, as shown Fig. S5. Scratch tests revealed the improved adhesion were about 10 N between the multilayer ta-C films and the substrate, while the single layer ta-C films easily peeled off from the substrate (shown in Supplementary file). High stress generally leads to weak adhesion of the single layer ta-C film on the YG6 substrate. The residual stress test results (Fig. S6) revealed that the S-1 film possessed a high value exceeding 10 GPa, leading to the occurrence of extensive spalling and fragments. The decreased values of 8.2, 7.6, 6.2 GPa were obtained for the M-1, M-2, M-3 film, respectively. The periodically introduced low-sp³-content layers are susceptible to plastic deformation, which could act as cushion to relieve the stress. Besides, the interfaces could play an important role in stress relief by absorbing energy and restrain initiation and propagation of cracks [30–32]. Therefore it can be concluded that the designed multilayer structure effectively reduced the residual stress and restrained spalling of the ta-C films. Therefore, the following studies are focused on the multilayer ta-C film system.

XPS depth profiling was carried out to elucidate the evolution of sp³ and sp² content in multilayer system. Typical deconvolution of the C 1s spectrum of the M-3 film at different etching time are demonstrated in Fig. 3(a) and (b). The sp³ content at the etching time of 600 s and 3120 s is 58.5% and 43.1%, respectively, which clearly confirms the variation of sp³ content at different depth of the film. Fig. 3(c) further exhibits the relative content of sp³ and sp² carbon atoms as a function of etching time. There is a sp²-rich layer on the top surface of the film until etching to 300 s. Then, a modulation of sp³ content emerges, in which high sp³ content is alternated by low sp³ content. In Fig. 3(c), the interface is defined when sp³ content equals to the sp² content. Including the top sp²-rich layer, six individual layers can be identified, as illustrated by different background colors. High hardness of ta-C films led to weak etching effect of argon ion, so the depth profile only proceeded to six layers. The sp³ content of the individual layer in multilayer system deviates from the corresponding single layers, which could be ascribed to the influence of stress or strain field in the multilayer film [33]. These results prove that multilayer structure with different sp³ content can be obtained by adjusting the bias voltage.

The TEM cross-sectional image of the M-3 film on silicon substrate are exhibited in Fig. 4(a). Alternate dark and bright layer could be

obviously observed due to density variation. The bright layer corresponds to the low-sp³-content layer deposited at −350 V, while the dark layer is the high-sp³-content layer deposited at −50 V. Due to the influence of platinum protective layer, only seven layers can be distinguished. The first layer in contact with the silicon substrate is relatively thicker due to a combination of pre-deposited ta-C by arc etching and the first soft layer deposited at −50 V. The total thickness is ~260 nm measured from the TEM cross-sectional image, which is consistent with experimental design. Fig. 4(b) displays the enlarged image of the multilayer structure. The thickness of high-sp³-content and low-sp³-content layer is 30 nm and 40 nm, respectively. HRTEM image in Fig. 4(c) demonstrates the formation of a mixed Si/ta-C interface layer, due to the impingement of high energy carbon ions into the substrate. HRTEM images also testify the amorphous structure of ta-C film.

STEM image and EELS spectra were employed to access the local carbon bonding. Taking the M-3 film as an example, obvious multilayer structure was observed in STEM image, as shown in Fig. 5(a). The variation of contrast may be due to the difference of sublayer density. High resolution EELS spectra were obtained at different locations (different sublayers) in STEM image, which was labelled as a-g. HOPG was served as a standard. The processed C-K edge spectra are presented in Fig. 5(b). The π* peak centered at 285 eV is fitted with a Gaussian function, while the σ* peak is integrated within the small energy window from 290 to 305 eV. The fraction of sp² bonded carbon atoms x is given by [34,35]

$$\frac{(\pi * / \sigma *)_{film}}{(\pi * / \sigma *)_{standard}} = \frac{3 - x}{4x} \tag{2}$$

The calculated carbon bond fractions for different EELS position are showed in Fig. 5(c). The contents of sp² and sp³ hybridized carbon atoms in adjacent sublayers are effectively modulated, showing a periodic oscillation of sp³ content between 40% and 60%. The EELS results confirm the existence of alternating multilayered structures with high and low sp³ content, which is consistent with XPS depth profiling.

3.2. Tribological properties

Friction coefficient curves against sliding times are presented in Fig. 6(a). It can be noted that the friction coefficient of YG6 substrate is higher than 0.3, and the friction coefficient curve exhibits a high fluctuation, while the multilayer ta-C film coated YG6 samples have smooth curves and much lower friction coefficient between 0.06 and 0.08, exhibiting good lubricant effect. The average friction coefficient and the wear rate calculated according to the cross-section profile of the wear tracks are exhibited in Fig. 6(b). The M-1 film has the lowest friction coefficient of 0.06, while the M-2 and M-3 films obtain the same value of 0.08. Moreover, the lowest wear rate of 2.87 × 10⁻⁷ mm³/Nm is obtained by the M-1 film, while the YG6 substrate possesses a highest value of 6.14 × 10⁻⁷ mm³/Nm. After coated with the multilayer ta-C films, the wear rate decreased 34% to 50%. The above results justify the good lubrication and anti-wear effect of the prepared multilayer ta-C films.

SEM morphology and cross-section profile of wear tracks are shown in Fig. 7. YG6 substrate possesses the widest wear track and a large
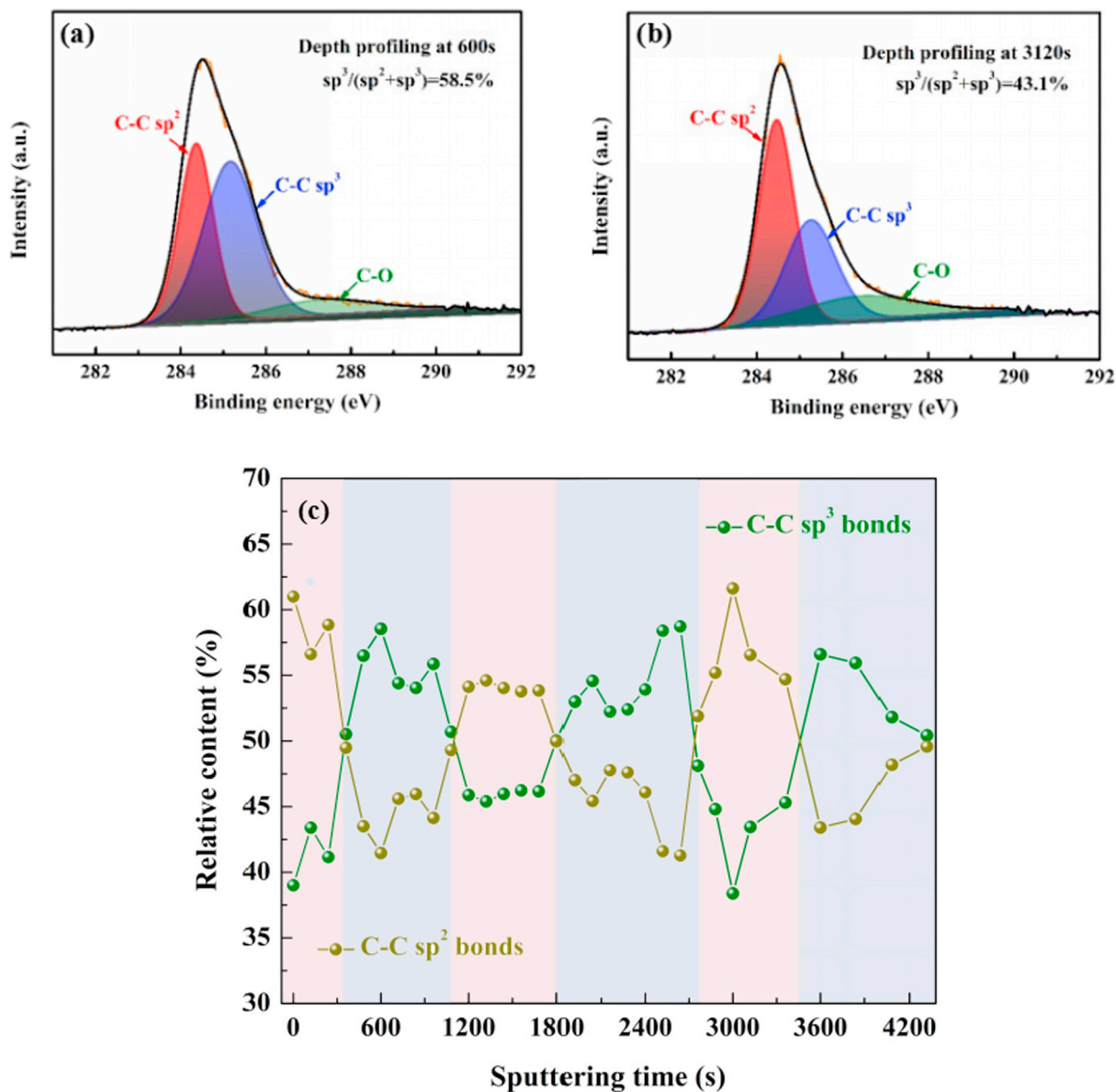
Fig. 3. Typical deconvolution of the C 1s spectra at etching time 600 s (a) and 3120 s (b) and XPS depth profiling scheme (c) of the M-3 film.
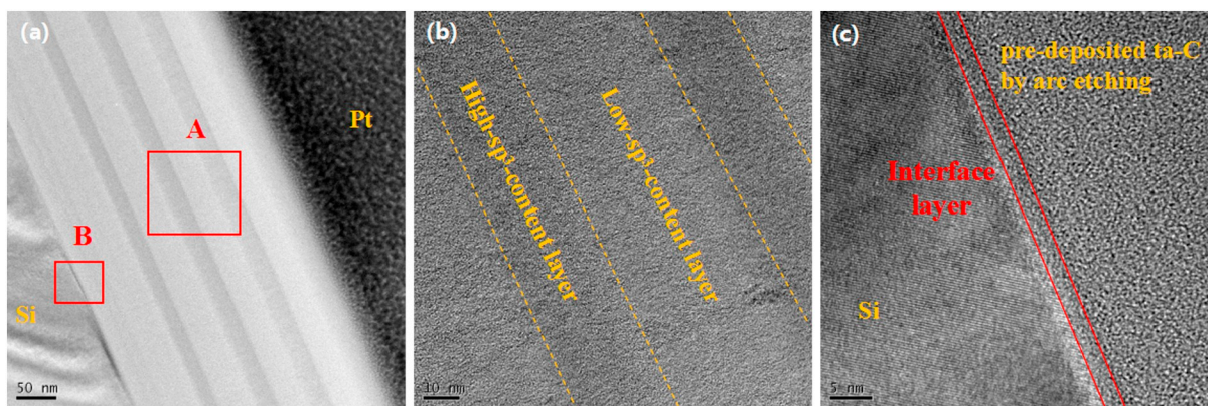

Fig. 4. TEM cross section image (a), HRTEM image of region A (b) and B (c) of M-3 film.

amount of debris, indicating the poor wear resistance. On the contrary, narrowed wear tracks are observed for the multilayer ta-C film coated YG6 substrates, in which M-1 film coated one has the narrowest and shallowest wear track.

In order to understand the friction mechanism, Raman tests were conducted to detect the wear products. Fig. 8 shows the Raman spectra
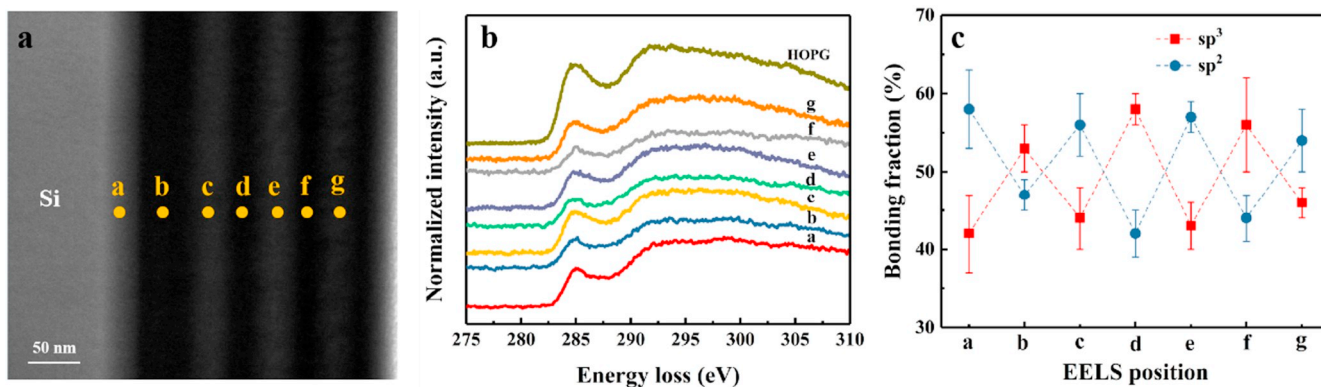
Fig. 5. STEM image of the M-3 film (a) and the C-K edge spectra obtained from different locations in the STEM image, labelled as a-g, and HOPG (b), calculated carbon bond fractions for different EELS position (c).
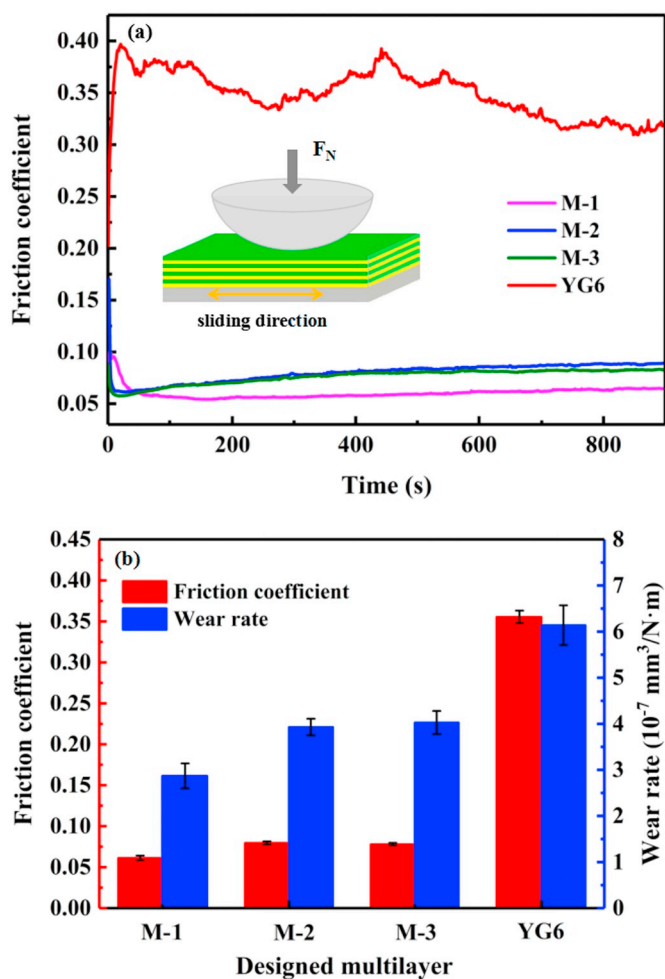

Fig. 6. (a) Friction coefficient curves against sliding times (the inset is schematic diagram of friction test), (b) average friction coefficient and wear rate of multilayer ta-C films coated and uncoated YG6.

of original ta-C films and their corresponding wear tracks. All spectra exhibit a broad asymmetric Raman peak in a wavenumber range from $1000\,cm^{-1}$ to $1800\,cm^{-1}$, indicating the typical characteristics of amorphous carbon. Typically, Raman spectra of amorphous carbon is composed of D peak and G peak, which locate at $1350\,cm^{-1}$ and $1580\,cm^{-1}$, respectively. After Gaussian fitting, the area ratio of D peak and G peak are calculated, which is referred as I_D/I_G ratio. The evolution of I_D/I_G ratio could shed light on the friction mechanism. The I_D/I_G

ratio of the deposited ta-C is 0.54, then increases to 0.62 in the middle of wear track, and reaches the maximum of 1.26 in tail area. The increased I_D/I_G ratio reveals an increasing number of sp^2 clusters, which indicates that graphitization occurred in the contact interface during friction. However, no Raman signal of amorphous carbon could be detected on the wear scar of the Al_2O_3 counterpart, suggesting that no obvious transfer layer was formed. At the same time, Al_2O_3 is intrinsically chemical inert, leading to the weak interaction across the sliding interface [36]. As a result, the weak interaction between graphitization component and grinding ball leads to good antifriction performance.

In addition, it is worth noting that the passivation of dangling bonds of ta-C film could work. Those dangling bonds existed in contacting interface would be passivated by chemically active molecules such as water and oxygen, which are abundant in atmospheric environment. Deactivation of dangling bonds further weakens the adhesion of frictional pairs and thereby yields low friction coefficient and good wear resistance [37,38].

At present, few studies have elucidated the origin of difference in anti-wear behavior of different multilayer DLC films consisting of sp^2-rich DLC layer (soft layer) and sp^3-rich DLC layer (hard layer). Xu et al. [25] and Lin et al. [31] both presented that the best wear resistance of multilayer DLC film was attributed to a balance between hardness and residual stress. Zhang et al. [30] found that high toughness is consistent with high wear resistance for multilayer DLC films, due to inhibition of abrasive wear and contribution to the formation of a graphitized transfer film. However, our experimental results are inconsistent with the above standpoints.

In principle, the wear behavior of DLC film is closely related to test conditions and its intrinsic properties. Considering the same friction test parameters and counterpart ball, the difference in wear resistance between M-1, M-2, M-3 film is mainly ascribed to the characteristics of the film itself. The hardness and Young's modulus, supplied in Fig. S7, show a decreasing trend for M-1, M-2, M-3 film. The correlation between the sp^3 content and hardness has been verified by numerous researches [9,39]. As a result, it is rational that the mechanical properties will be dominated by the soft sub-layer since the hard sub-layer is fixed. The highest hardness of 54.6 GPa and the highest Young's modulus of 693.5 GPa was obtained in the M-1 film.

During friction, high hardness provides superior load carrying capacity and contributes to the decreased depth of wear track, which is evidenced by narrower and shallower wear track of M-1 film (Fig. 7). Moreover, the ratio of hardness and elastic modulus (H/E), which is associated with the elastic strain to failure, plays an important role in determining the limit of elastic behavior in a surface contact and then clearly affects the wear performance [40]. In this work, hardness and H/E ratios are employed to analyze the wear behaviors between different samples, as shown in Fig. 9. The hardness exhibits similar trends
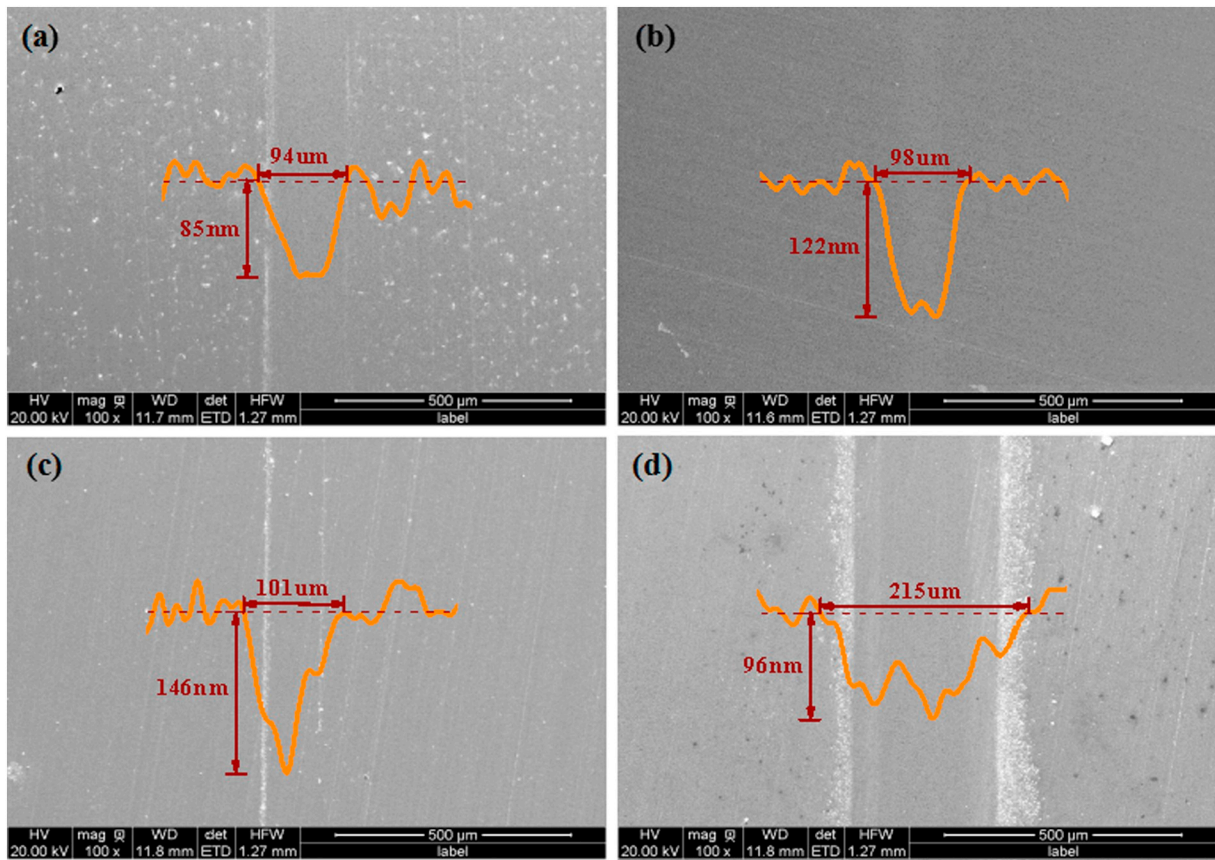
Fig. 7. Surface and cross-section profile of wear tracks M-1(a); M-2(b); M-3(c); YG6(d).
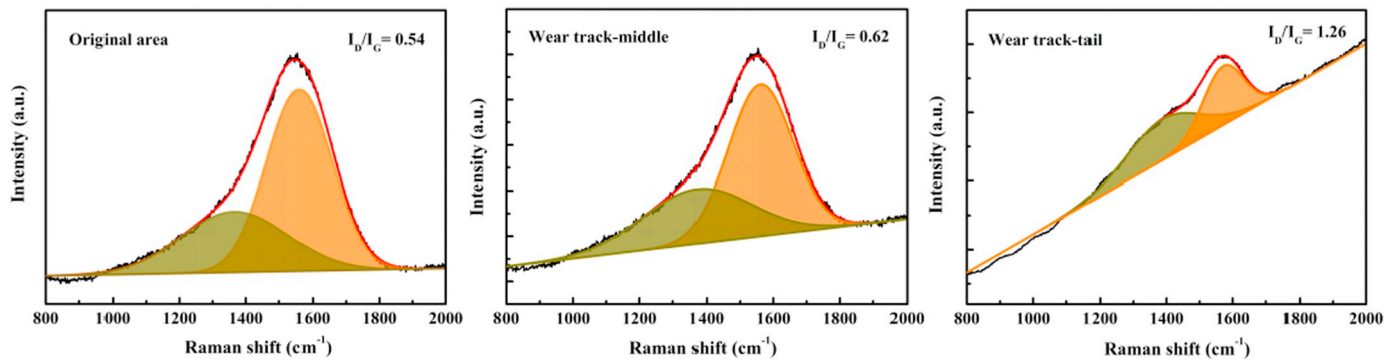

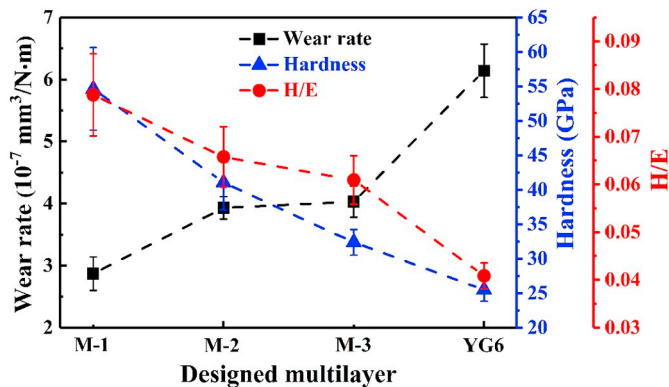**Fig. 8.** Raman spectrums of original area and wear track area.

Fig. 9. Relationship between wear rate, hardness and H/E ratio.

with the wear rate, suggesting the beneficial effect of high hardness to wear resistance. In contrast to the hardness, the wear rate is mainly in inverse proportion to H/E ratio, which means a high H/E ratio indicates good wear resistance of multilayer ta-C film. Many researchers have shed on the relationship between H/E ratio and wear behavior [41–43]. Cai et al. [43] and Bai et al. [44] concluded that higher H/E ratio indicates enhanced wear resistance of a-C/a-C:Ti multilayer films. Pei et al. [45] suggested that the wear rate of TiC/a-C:H nanocomposite coatings significantly decreases with increase in hardness and especially with increasing the H/E ratio. Maruno et al. [46] demonstrated that improving the wear resistance required high plastic index parameter (H/E) values rather than high H values. Considering our friction results, a high H/E ratio indicates good wear resistance of multilayer ta-C film, which provides guidance for evaluating the wear performances of materials.
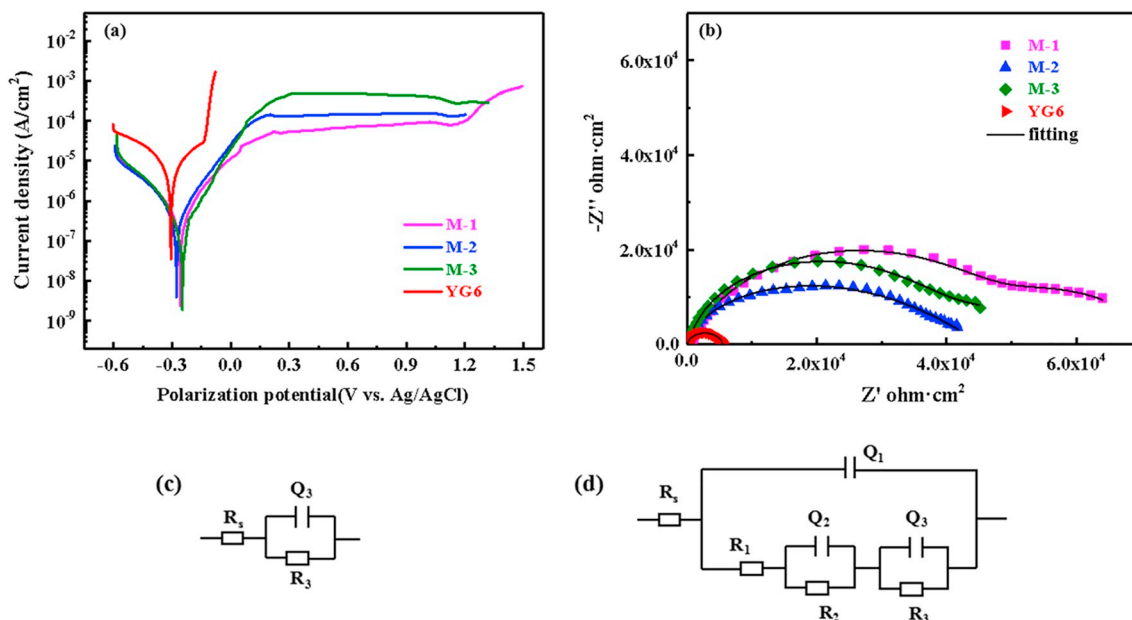
Fig. 10. (a) Potentiodynamic polarization curves, (b) Nyquist plots, (c) and (d) equivalent circuit model of multilayer ta-C coated and uncoated YG6.

3.3. Electrochemical corrosion behaviors

To elucidate the effects of multilayer structure on electrochemical corrosion performance of the multilayer ta-C films, electrochemical corrosion tests were conducted in 3.5 wt% NaCl solution. Fig. 10(a) presents the potentiodynamic polarization curves of multilayer ta-C film coated and uncoated YG6 cemented carbide substrate. For the YG6 substrate, the corrosion current density maintains a high level during the whole potentiodynamic scanning. Even worse, pitting corrosion occurred at about −0.14 V, revealing poor intrinsic corrosion resistance of the YG6 substrate. The surface deposition of ta-C film improves the corrosion resistance and retards the occurrence of pitting corrosion. For multilayer ta-C coated samples, adjusting the component of adjacent layer leads to little difference on polarization behavior. The cathode branch of the potentiodynamic polarization curves nearly coincides with each other, while the anode branch differs a little, indicating that similar electrode reaction occurs during the test.

The corrosion current density (i_{corr}) and corrosion potential (E_{corr}) deduced from potentiodynamic polarization curves through Tafel fitting are summarized in Table 2. It shows that E_{corr} of the multilayer ta-C coated sample shifts towards noble direction in 3.5 wt% NaCl solution compared to the YG6 substrate, indicating the decreased corrosion tendency. Moreover, i_{corr} reduces by about 10 times and the M-1 film obtains the lowest corrosion current density of 2.19×10^{-8} A/cm², further revealing the improved corrosion resistance.

Fig. 10(b) shows the Nyquist plots of multilayer ta-C coated and uncoated YG6. The YG6 substrate shows only one semicircle, while at least two distinct semicircles could be observed for the ta-C coated samples. Multilayer ta-C films significantly increase the arc radius compared to the YG6 substrate, while the M-1 film has the largest arc radius. Large arc radius suggests superior corrosion resistance.

Therefore, the deposition of the multilayer ta-C films provides good corrosion protection to the YG6 substrate.

Impedance data obtained from EIS test are fitted with equivalent circuit (EC), in order to analyze the physical process taking place in the system. Two different equivalent circuit models presented in Fig. 10(c) and (d) are established to fit the EIS data of uncoated and multilayer ta-C coated YG6, respectively. The EC diagram of the YG6 substrate, labelled as $R_s(Q_3R_3)$, possessed one time constant in which R_1, R_3, Q_3 represent the solution resistance, the charge transfer resistance and double layer capacitance, respectively. With respect to the multilayer ta-C coated YG6 samples, an equivalent circuit $R_s(Q_1(R_1(Q_2R_2)(Q_3R_3)))$ with three time constants is employed to simulate the EIS data. In this circuit, R_s corresponds to solution resistance, R_1 and Q_1 are related to pore resistance and its capacitance, stemming from microdefects (e.g., pinhole, inclusion, dimple) existed in amorphous ta-C film. These microdefects could act as active sites for corrosion, leading to aggravated penetration of corrosive electrolyte solutions. R_2 and Q_2 are associated with the resistance and capacitance of the ta-C barrier layer. Similarly, R_3 and Q_3 represent the charge transfer resistance and double layer capacitance of the interface between the substrate and the film. The fitting results are showed in Table 3.

It can be noted that the values of R_1 are relatively small ($63.90–740.6 \,\Omega\,cm^{-2}$). This phenomenon could be attributed to the existence of microdefects. The polarization resistance R_p evaluated by the sum of R_1, R_2 and R_3 is proposed to evaluate the corrosion resistance of different samples. The YG6 substrate just has a charge

Table 2
Summary of E_{corr} and I_{corr} values from the polarization curves.

Sample	E_{corr} (V, vs Ag/AgCl)	i_{corr} (A/cm²)
M-1	−0.257	2.19×10^{-8}
M-2	−0.265	2.71×10^{-8}
M-3	−0.243	2.81×10^{-8}
YG6	−0.305	2.20×10^{-7}

Table 3
Fitted parameters deduced from EIS data using equivalent circuits.

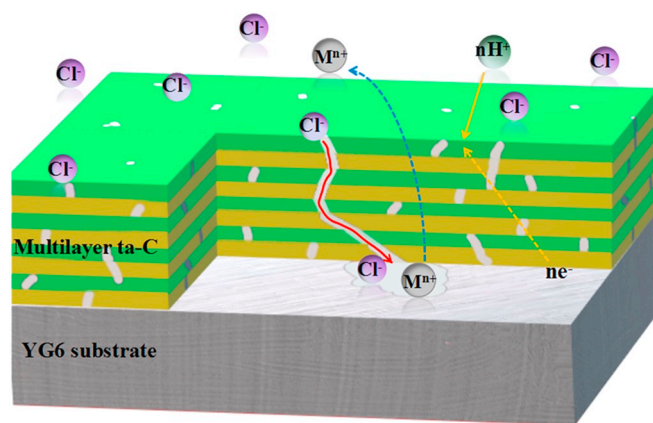|	M-1	M-2	M-3	YG6
R_s ($\Omega\,cm^{-2}$)	27.86	32.01	46.52	49.50
Y_1 ($\Omega^{-2}\,cm^{-2}\,S^{-n}$)	2.76×10^{-7}	9.09×10^{-6}	9.10×10^{-6}	–
n_1	0.79	0.50	0.84	–
R_1 ($\Omega\,cm^{-2}$)	740.60	63.90	333.70	–
Y_2 ($\Omega^{-2}\,cm^{-2}\,S^{-n}$)	1.97×10^{-4}	1.83×10^{-6}	8.18×10^{-6}	–
n_2	0.81	1.00	1.00	–
R_2 ($\Omega\,cm^{-2}$)	2.36×10^4	4.50×10^4	3.53×10^4	–
Y_3 ($\Omega^{-2}\,cm^{-2}\,S^{-n}$)	5.44×10^{-6}	1.30×10^{-5}	1.92×10^{-4}	2.73×10^{-5}
n_3	0.85	0.93	0.49	0.92
R_3 ($\Omega\,cm^{-2}$)	4.76×10^4	188.10	3.03×10^4	5.45×10^3
χ^2	3.93×10^{-4}	3.23×10^{-4}	4.69×10^{-4}	1.54×10^{-3}

Fig. 11. A schematic diagram of the corrosive behavior of multilayer ta-C film coated YG6.

transfer resistance of $5.45 \times 10^3 \, \Omega \, cm^{-2}$. The R_p values for M-1, M-2, M-3 films are 7.19×10^4, 4.52×10^4, and $6.59 \times 10^4 \, \Omega \, cm^{-2}$, respectively. The M-1 film exhibited superior corrosion resistance to the M-2 and M-3 films, which might be attributed to the higher sp^3 content of the soft-layer in the multilayer structure. The corrosion solution could penetrate into the multilayer system due to the existence of through-hole defects as revealed by the small pore resistance. Under these circumstances, ta-C sub-layers with higher sp^3 content have lower corrosion tendency, thus providing better corrosion resistance [47,48]. As a whole, the results clearly confirm that the corrosion resistance of YG6 in 3.5 wt% NaCl solution is effectively improved by the multilayer ta-C films, although adjusting the composition of the adjacent layer has little effect on the electrochemical corrosion performance.

A schematic diagram of corrosive behavior of the multilayer ta-C film coated YG6 is presented Fig. 11. As discussed above, multilayer ta-C film provides good corrosion resistance to cemented carbide substrate, which could be attributed to the good barrier effect and insulating property of the amorphous ta-C film. Meanwhile, the multilayer structure introduces new interfaces, leading to deterrence of penetration of the corrosive media. On the other hand, EIS results, as an effective tool to elucidate the holes and defects in films [49–51], clearly demonstrate small values of pore resistance in the multilayer ta-C system. Besides, the equivalent circuit employed for ta-C coated sample is in accordance with studies concerning micro-arc oxidation and surface porous materials, also confirming the existence of some extent of through-holes and defects [51,52]. These holes could act as fast diffusion channels for corrosive ions such as chloride ions, triggering the electrochemical corrosion of substrate. As a result, the through-holes limit the electrochemical corrosion protection performance and result in the indistinguishable electrochemical behavior of different multilayer ta-C films.

4. Conclusions

The multilayer ta-C films with alternating high and low sp^3 content were prepared by a facile method through periodically adjusting the bias voltage. It was found that the mechanical and tribological properties could be tailored by varying sp^3 content of the individual layers. The M-1 film had the lowest friction coefficient of 0.06 and the lowest wear rate of $2.87 \times 10^{-7} \, mm^3/Nm$. The wear rate of multilayer ta-C film was in inverse proportion to H/E ratio, which means that a high H/E ratio indicates good wear resistance. The graphitization and surface passivation were responsible for the antifriction effect of multilayer ta-C films.

Electrochemical tests confirmed the good corrosion protection provided by the multilayer ta-C films. However, adjusting the composition of the adjacent layer had little effect on the electrochemical

corrosion performance. Effective strategies to restrain pinholes and defects in the ta-C films are needed to further improve the corrosion resistance in 3.5 wt% NaCl solution.

Appendix A. Supplementary data

Supplementary data to this article can be found online at https://doi.org/10.1016/j.surfcoat.2019.05.087.

References

[1] R.J.K. Wood, Marine wear and tribocorrosion, Wear 376–377 (2017) 893–910.
[2] W.Q. Bai, Y.J. Xie, L.L. Li, X.L. Wang, C.D. Gu, J.P. Tu, Tribological and corrosion behaviors of Zr-doped graphite-like carbon nanostructured coatings on Ti6Al4V alloy, Surf. Coat. Technol. 320 (2017) 235–239.
[3] B.S. Lou, J.W. Lee, C.M. Tseng, Y.Y. Lin, C.A. Yen, Mechanical property and corrosion resistance evaluation of AZ31 magnesium alloys by plasma electrolytic oxidation treatment: effect of MoS 2 particle addition, Surf. Coat. Technol. 350 (2018) 813–822.
[4] Y. Gu, X. Zheng, L. Qi, H. Ma, Z. Lei, D. Yang, Investigating corrosion performance and corrosive wear behavior of sol–gel/MAO-coated Mg alloy, Tribol. Lett. 66 (2018) 101.
[5] Y. Ye, Y. Wang, X. Ma, D. Zhang, L. Wang, X. Li, Tribocorrosion behaviors of multilayer PVD DLC coated 304L stainless steel in seawater, Diam. Relat. Mater. 79 (2017) 70–78.
[6] M. Azzi, M. Paquette, J.A. Szpunar, J.E. Klemberg-Sapieha, L. Martinu, Tribocorrosion behaviour of DLC-coated 316L stainless steel, Wear 267 (2009) 860–866.
[7] G.H. Zhao, R.E. Aune, N. Espallargas, Tribocorrosion studies of metallic biomaterials: the effect of plasma nitriding and DLC surface modifications, J. Mech. Behav. Biomed. Mater. 63 (2016) 100–114.
[8] R. Bayón, A. Igartua, J.J. González, U.R.D. Gopegui, Influence of the carbon content on the corrosion and tribocorrosion performance of Ti-DLC coatings for biomedical alloys, Tribol. Int. 88 (2015) 115–125.
[9] J. Robertson, Diamond-like amorphous carbon, Mater. Sci. Eng. R 37 (2002) 129–281.
[10] Y. Fujii, T. Imai, Y. Miyamoto, N. Ueda, M. Hosoo, T. Harigai, Y. Suda, H. Takikawa, H. Tanoue, M. Kamiya, M. Taki, Y. Hasegawa, N. Tsuji, S. Kaneko, Dry machining of metal using an engraving cutter coated with a droplet-free ta-C film prepared via a T-shape filtered arc deposition, Surf. Coat. Technol. 307 (2016) 1029–1033.
[11] F. Präßler, W. Grimm, T. Chudoba, Properties of ta-C films for tools and machinery parts, Plasma Process. Polym. 6 (2010) S468–S472.
[12] M.C. Kang, H.S. Tak, Y.K. Jeong, H.W. Lee, J.S. Kim, Properties and tool performance of ta-C films deposited by double-bend filtered cathodic vacuum arc for micro drilling applications, Diam. Relat. Mater. 19 (2010) 866–869.
[13] R. Paul, Uniformly dispersed nanocrystalline silver reduces the residual stress within diamond-like carbon hard coatings, Nano-Struct. Nano-Objects 10 (2017) 69–79.
[14] C. Hong, J. Tu, C. Gu, X. Zheng, D. Liu, R. Li, S.X. Mao, The effect of stress relaxation on the microstructure and hardness evolution of pure amorphous-carbon and C/Ti multilayer films, Adv. Eng. Mater. 12 (2010) 920–925.
[15] C. Wei, Y.S. Wang, F.C. Tai, The role of metal interlayer on thermal stress, film structure, wettability and hydrogen content for diamond like carbon films on different substrate, Diam. Relat. Mater. 18 (2009) 407–412.
[16] C.S. Lee, K.R. Lee, S.H. Suh, Mechanical property optimisation of materials by nanostructuring: reduction of residual compressive stress in ta-C film, Mater. Sci. Technol. 20 (2004) 993–995.
[17] F. Wen, N. Huang, F.J. Jing, H. Sun, Y. Cao, Effects of negative bias voltage on structure and mechanical properties of DLC films synthesized by FCVA deposition, Adv. Mater. Res. 287-290 (2011) 2203–2206.
[18] G.M. Pharr, D.L. Callahan, S.D. Mcadams, T.Y. Tsui, S. Anders, A. Anders, J.W.A. Iii, I.G. Brown, C.S. Bhatia, S.R.P. Silva, Hardness, elastic modulus, and structure of very hard carbon films produced by cathodic-arc deposition with substrate pulse biasing, Appl. Phys. Lett. 68 (1996) 779–781.
[19] J.Y. Jao, S. Han, C.C. Yen, Y.C. Liu, L.S. Chang, C.L. Chang, H.C. Shih, Bias voltage effect on the structure and property of the (Ti:Cu)-DLC films fabricated by cathodic arc plasma, Diam. Relat. Mater. 20 (2011) 123–129.
[20] J. Zhu, J. Han, X. Han, H.I. Schlaberg, J. Wang, sp3-rich deposition conditions and growth mechanism of tetrahedral amorphous carbon films deposited using filtered arc, J. Appl. Phys. 104 (2008) 013512.
[21] P.J. Fallon, V.S. Veerasamy, C.A. Davis, J. Robertson, G.A. Amaratunga, W.I. Milne,

J. Koskinen, Properties of filtered-ion-beam-deposited diamondlike carbon as a function of ion energy, Phys. Rev. B 48 (1993) 4777–4782.

[22] O.S. Panwar, M.A. Khan, M. Kumar, S.M. Shivaprasad, B.S. Satyanarayana, P.N. Dixit, R. Bhattacharyya, M.Y. Khan, Effect of high substrate bias and hydrogen and nitrogen incorporation on filtered cathodic vacuum arc deposited tetrahedral amorphous carbon films, Thin Solid Films 516 (2008) 2331–2340.

[23] V. Zavaleyev, J. Walkowicz, Influence of the substrate bias potential on the properties of ta-C coatings deposited using Venetian blind plasma filter, Thin Solid Films 581 (2014) 32–38.

[24] X. Yu, X. Zhang, C.B. Wang, M. Hua, L.G. Wang, A tribological study of tetrahedral amorphous carbon films prepared by filtered cathodic vacuum arc technique, Vacuum 75 (2004) 231–236.

[25] Z. Xu, Y.J. Zheng, F. Jiang, Y.X. Leng, H. Sun, N. Huang, The microstructure and mechanical properties of multilayer diamond-like carbon films with different modulation ratios, Appl. Surf. Sci. 264 (2013) 207–212.

[26] Z.Y. Xu, Y.J. Zheng, H. Sun, Y.X. Leng, N. Huang, Numerical and experimental study of residual stress of multilayer diamond-like carbon films prepared by filtered cathodic vacuum arc deposition, IEEE Trans. Plasma Sci. 40 (2012) 2261–2266.

[27] G.G. Wang, H.Y. Zhang, W.Y. Li, F.X. Yang, L. Cui, H.B. Zuo, J.C. Han, The preparation and evaluation of graded multilayer ta-C films deposited by FCVA method, Appl. Surf. Sci. 257 (2011) 5064–5069.

[28] X. Han, J. Zhu, J. Han, M. Tan, Z. Jia, C. Jiang, Stress, mechanical and adhesion properties of multilayer tetrahedral amorphous carbon films, Appl. Surf. Sci. 255 (2008) 607–609.

[29] C.K. Park, S.M. Chang, H.S. Uhm, S.H. Seo, J.S. Park, XPS and XRR studies on microstructures and interfaces of DLC films deposited by FCVA method, Thin Solid Films 420 (2002) 235–240.

[30] Y. Zhang, Y. Zhai, F. Li, S. Zhang, P. Zhang, S. Zhang, Effect of microstructure and mechanical properties difference between sub-layers on the performance of alternate hard and soft diamond-like carbon multilayer films, Surf. Coat. Technol. 232 (2013) 575–581.

[31] Y. Lin, A.W. Zia, Z. Zhou, P.W. Shum, K.Y. Li, Development of diamond-like carbon (DLC) coatings with alternate soft and hard multilayer architecture for enhancing wear performance at high contact stress, Surf. Coat. Technol. 320 (2017) 7–12.

[32] M. Gioti, S. Logothetidis, C. Charitidis, Stress relaxation and stability in thick amorphous carbon films deposited in layer structure, Appl. Phys. Lett. 73 (1998) 184–186.

[33] J. Pu, J. Wang, D. He, S. Wan, Corrosion and tribocorrosion behaviour of superthick diamond-like carbon films deposited on stainless steel in NaCl solution, Surf. Interface Anal. 48 (2016) 360–367.

[34] J.J. Cuomo, J.P. Doyle, J. Bruley, J.C. Liu, Sputter deposition of dense diamond-like carbon films at low temperature, Appl. Phys. Lett. 58 (1991) 466.

[35] J. Xie, K. Komvopoulos, The effect of argon ion irradiation on the thickness and structure of ultrathin amorphous carbon films, J. Appl. Phys. 119 (2016) 095304.

[36] L. Cui, Z. Lu, L. Wang, Toward low friction in high vacuum for hydrogenated diamondlike carbon by tailoring sliding interface, ACS Appl. Mater. Interfaces 5 (2013) 5889–5893.

[37] J. Andersson, R.A. Erck, A. Erdemir, Friction of diamond-like carbon films in different atmospheres, Wear 254 (2003) 1070–1075.

[38] L. Wang, L. Cui, Z. Lu, H. Zhou, Understanding the unusual friction behavior of hydrogen-free diamond-like carbon films in oxygen atmosphere by first-principles calculations, Carbon 100 (2016) 556–563.

[39] R. Bayón, A. Igartua, X. Fernández, R. Martínez, R.J. Rodríguez, J.A. García, A.D. Frutos, M.A. Arenas, J.D. Damborenea, Corrosion-wear behaviour of PVD Cr/CrN multilayer coatings for gear applications, Tribol. Int. 42 (2009) 591–599.

[40] A. Leyland, A. Matthews, On the significance of the H/E ratio in wear control: a nanocomposite coating approach to optimised tribological behaviour, Wear 246 (2000) 1–11.

[41] W.Q. Bai, X.L. Wang, C.D. Gu, J.P. Tu, Influence of duty cycle on microstructure, tribological and corrosion behaviors of a-C/a-C:Ti multilayer films, Thin Solid Films 584 (2015) 214–221.

[42] M. Łępicka, M. Grądzka-Dahlke, D. Pieniak, K. Pasierbiewicz, A. Niewczas, Effect of mechanical properties of substrate and coating on wear performance of TiN- or DLC-coated 316LVM stainless steel, Wear 382-383 (2017) 62–70.

[43] J.B. Cai, X.L. Wang, W.Q. Bai, D.H. Wang, C.D. Gu, J.P. Tu, Microstructure, mechanical and tribological properties of a-C/a-C:Ti nanomultilayer film, Surf. Coat. Technol. 232 (2013) 403–411.

[44] W.Q. Bai, J.B. Cai, X.L. Wang, D.H. Wang, C.D. Gu, J.P. Tu, Mechanical and tribological properties of a-C/a-C:Ti multilayer films with various bilayer periods, Thin Solid Films 558 (2014) 176–183.

[45] Y.T. Pei, D. Galvan, J.T.M.D. Hosson, C. Strondl, Advanced TiC/a-C:H nanocomposite coatings deposited by magnetron sputtering, J. Eur. Ceram. Soc. 26 (2006) 565–570.

[46] A.N. Hidenobu Marunoa, Adhesion and durability of multi-interlayered diamond-like carbon films deposited on aluminum alloy, Surf. Coat. Technol. 354 (2018) 134–144.

[47] Y.J. Xu, J. Zhang, J.R. Shi, R. Ji, J.P. Wang, The effect of carbon structure on in-situ protection for granular thin film media, Tribol. Int. 36 (2003) 325–328.

[48] Ho-Gun Kim, Seung-Ho Ahn, Jung-Gu Kim, Se Jun Park, Kwang-Ryeol Lee, Effect of Si-incorporation on wear–corrosion properties of diamond-like carbon films, Thin Solid Films 482 (2005) 299–304.

[49] S.H. Ahn, J.H. Lee, H.G. Kim, J.G. Kim, A study on the quantitative determination of through-coating porosity in PVD-grown coatings, Appl. Surf. Sci. 233 (2004) 105–114.

[50] A. Shanaghi, A. Rouhaghdam, Effects of duty cycle on microstructure and corrosion behavior of TiC coatings prepared by DC pulsed plasma CVD, Appl. Surf. Sci. 258 (2012) 3051–3057.

[51] A. Zeng, E. Liu, I.F. Annergren, S.N. Tan, S. Zhang, P. Hing, J. Gao, EIS capacitance diagnosis of nanoporosity effect on the corrosion protection of DLC films, Diam. Relat. Mater. 11 (2002) 160–168.

[52] H. Wu, S. Xiao, D. Chen, A.M. Qasim, K. Ding, G. Wu, P.K. Chu, Effects of diamond-like carbon film on the corrosion behavior of NdFeB permanent magnet, Surf. Coat. Technol. 312 (2017) 66–74.